IEEE Access
Multidisciplinary | Rapid Review | Open Access Journal

Received March 20, 2019, accepted April 11, 2019, date of publication April 23, 2019, date of current version May 2, 2019.

Digital Object Identifier 10.1109/ACCESS.2019.2912807

Cropland Mapping and Change Detection: Toward Zimbabwean Cropland Inventory

JULIANA USEYA, SHENGBO CHEN, AND MIKE MUREFU

Department of Remote Sensing and GIS, College of Geo-Exploration Science and Technology, Jilin University, Changchun 130026, China

Corresponding authors: Juliana Useya (julieuseya@yahoo.co.uk) and Shengbo Chen (chensb@jlu.edu.cn)

This work was supported in part by the Fundamental Research Funds for the Central Universities, China, through the Program for JLU Science and Technology Innovative Research Team under Grant 2017TD-26, in part by the Plan for Changbai Mountain Scholars of Jilin Province, China, under Grant JJLZ[2015]54, and in part by the Jilin Province and Jilin University Co-Building Project: Application and demonstration of Satellite Remote Sensing in Crop Planting Structure Adjustment Research under Grant SXGJXX2017-2.

ABSTRACT Accurate and spatially explicit cropland maps are crucial for many applications, which include sustainable crop monitoring, food security, and land and agriculture planning and management. Zimbabwe lacks reliable data on cropland extent of the old and new re-allocated areas for inventory purposes. Objectives of this paper are to map cropland utilizing: 1) automatic classification; 2) multi-classifier system (MCS); and 3) normalized difference vegetation index and bare-soil index (NDVI-BSI) thresholding and determine the spatiotemporal cropland changes. Change detection is implemented through a post-classification statistical method. The classified results are compared with SADC and ESA land cover products, GFSAD30AFCE cropland layer, and Google Earth imagery. Results reveal that MCS and NDVI-BSI performed the best and achieved overall accuracies of 80.54% and 79.32% for 2013, and for 2018, they attained accuracies of 87.90% and 88.56%, respectively. Automated classification, MCS, and NDVI-BSI thresholding produced average cropland areas of 3416396, 10346778, and 9788833 Ha, respectively. Visual assessment observations show that NDVI-BSI thresholding outperformed the other two techniques. Comparing further the MCS and NDVI-BSI thresholding approaches' results of total cropland areas of Zimbabwe's ten provinces for the years 2013 and 2018, coefficients of determination of 0.8404 and 0.9619, respectively, are achieved. Change detection shows a general increase in the cropland area due to human activities despite the prolonged drought. However, we recommend further exploration of NDVI-BSI threshold values to derive cropland layers since the method is robust and can be automated easily and faster without inputting training data. We also recommend simulation of the changes in cropland areas using cellular automata and/or agent-based modeling.

INDEX TERMS Bare-soil index (BSI), change detection, cropland, decision-level fusion, multi-classifier system, normalized difference vegetation index (NDVI).

I. INTRODUCTION

Agriculture and food are predominantly the world's major businesses, which are closely linked to sustainable development [1]. Most of the agricultural systems have to be transformed with aspirations to achieve global food security and environmental sustainability [2]. Global demand for food amongst other agricultural croplands' products is now a major driver of croplands and pastures expansion across much of the developing world [3]. The demand has increased at alarming rates during the past decades, whilst the agricultural land base needed for production has been shrinking in many parts of the world [2]–[4].

The world population is projected to reach 9.7 billion by 2050 [5], hence improved agricultural land production will be needed to meet such global demands. With the highest population growth rate, Africa is anticipated to account for more than half of the world's population between 2015 and 2050 hence resulting in escalation of per capita consumption rates [2], [4], [5].

As stated by the Food and Agriculture Organization (FAO) of the United Nations, croplands cover about 12% of Earth's ice-free land [2], [4]. Foley *et al.* [2] and Gibbs *et al.* [3] at some point indicated that agriculture was expanding mainly

The associate editor coordinating the review of this manuscript and approving it for publication was Dong Wang.

in the tropics, where about 80% of the new croplands were predicted to be substituting forests. Contrarily, Chen *et al.* [6] highlighted that over the past decade, rapid urbanization and forest plantations have caused large areas of cropland to shrink. Accurate knowledge and spatially explicit information on croplands distribution and changes can provide valued information crucial to understand activities taking place at the various locations which can influence policy making regarding sustainable food security, cropland management, food production and water resources [6]. Long term cropland inventories can support detection and improve understanding of cropland changes whether due to natural, climate change or human induced effects. Accurate maps showing cropland and non-cropland extent are the preliminary stage to developing higher-level products [7].

The world in general is awash in a heterogeneous spatial data gamut from satellite imagery, Unmanned Aerial Vehicle (UAV)-borne, airborne LiDAR to crowd sourced data [8], [9]. Endeavoring to efficiently monitor land cover/use changes, remote sensing techniques can provide reliable source of data for information extraction [10]. Satellite remote sensing has proved to be a cost-effective tool [11], [12] that has been widely implemented to determine croplands spatial distribution and extent over small and large regions. Due to the repetitive and synoptic coverages at relatively short, regular intervals, change detection became an imperative application of remote sensing [13] as well as monitoring and analyzing agricultural activities [14]. According to Ramankutty *et al.* [15], precise, current cropland distributions have been established from globally gridded land cover classification datasets. In contrast, Xiong *et al.* [7] argued that accurate and precise cropland extent maps at high spatial resolution over large areas such as continent or globe can be challenging to produce due to the smallholder dominant agricultural systems like those found in Africa and Asia.

Extraordinary potentials for remote sensing research and education have been brought to reality by the advent of generic, scalable cloud based geospatial computing image processing and multi-date platforms such as Google Earth Engine (GEE) [7], [16] or Amazon Web Services (AWS) [17]. Cloud computing is a method of remotely delivering and accessing information technology services and servers to store, manage and process data through web-based tools and applications [18], [19]. AWS provide a comprehensive and secure cloud services platform, offering compute power, database storage and analytics services in thirteen (13) regions across the world, and from 2015, the entire archive of Landsat 8 scenes was made publicly available [17], [18]. Machine Learning AWS also provide tools to build machine learning models, including data analysis, training and evaluation [18]. On the other hand, GEE contains over 200 public datasets, over 5 million images and more than 5 petabytes of data. GEE's suite of tools includes a collection of supervised classification algorithms (including Random Forest, CART and SVM) and workflows for building, training, applying and assessing classification algorithms.[1]

Cropland can be defined as arable land that is suitable for or used for crops production. The cropland in this paper refers to arable land comprising crop cultivated areas, fallows and plantations. Cropland is dynamic in nature hence the uniqueness of its characteristics compared to other land covers such as built-up, forest and pasture [20]. It undergoes various stages namely intensification, marginalization and abandonment [21]. Annually, cropland repeatedly perseveres preparation of fields, planting, growing and harvesting [20]. It is crucial to accurately map croplands and have up-to-date assessment of their spatial distribution. Azzali and Menenti, [22] successfully implemented NDVI time series to map vegetation types and soil and climate of Southern Africa, but the cropland class needed its own special approaches to map it rather than including it within the land use classes.

Focusing on the African continent, Xiong *et al.* [7] developed an automated methodology of mapping cropland in Africa using MODIS NDVI. Xiong *et al.* [23] mapped cropland extents at 30 m spatial resolution for African continent using Landsat 8 and Sentinel-2 imagery in GEE.

Hentze *et al.* [24] implemented MODIS time series data to map extent of cropland area in Zimbabwe focusing on former freehold tenure agricultural areas. However, their classification results underestimated the redistribution of farmland. Most of Zimbabwean cultivated fields are heterogeneous with small fragmented farms, hence accurate mapping requires imagery with high to moderate (30 – 250 m) spatial resolution and sophisticated approaches.

Limited research has been conducted related to the mapping of cropland areas in Zimbabwe as a whole. These few include amongst them Hentze *et al.* [24], who implemented MODIS NDVI time series. Most of the available cropland maps were derived from global and regional land cover products. The products do not necessarily target the agriculture component of the landscape and examples include ESA CCI-LC [25] GLC2000 [25], [26], GlobCover 2005/2009 [27], [28] and MODIS Land Cover [27], [29], Land cover datasets from University of Maryland and the World Land Cover dataset from the USGS EROS Data Centres Global Land Characteristics Database.

Furthermore, cropland class is frequently captured incongruously in such products since it has a dynamic status and due to the existence of diverse agro-systems, [27]. The products do not correctly account for specificities of some regions [30]. Waldner *et al.* [27] mentioned that cropland class is typically portrayed according to a land cover typology that focuses mainly on the natural vegetation types and is habitually contained within mosaic or mixed classes, making it difficult to use for agricultural applications (neither as an agricultural mask, nor as a source of information for crop-covered area). There are inevitable uncertainties when

[1] https://developers.google.com/earth-engine/classification

it comes to the croplands' extents, locations and their total areas extracted from the aforementioned land-use, land-cover (LULC) products, mainly due to the coarse spatial resolution of the map products.

Zhang and Roy [31] briefly underscored advantages of utilizing existing LULC maps as a source of training data. Wessels *et al.* [32] used land cover maps derived from 20 m SPOT5 images (EKZNW land cover maps) as training and validation datasets. Radoux *et al.* [33] developed an algorithm that automatically extracted training sample from Global Land Cover (GLC) 2000 map, Corine Land Cover (CLC) map and GLC 2000 for global land cover mapping using 300-m MERIS. Jia *et al.* [34] proposed an automatic way to update a land-cover map from a 30 m resolution (finer-resolution) global land-cover dataset initially produced by Gong *et al.* [35]. This research is aimed at exploring the automation of cropland mapping from MCD12Q1 LULC dataset and since it contains annual land cover maps, cropland changes can be determined.

Change detection analysis encompasses a wide assortment of processes utilized to identify, describe and quantify differences in the state of an object or phenomenon by observing it at different times but same location [10], [36]. It is vital for the sustainable development of economy and environment [4]. It is crucial to comprehend and characterize the dynamics occurring on croplands to assist in assessing food security scenarios at different levels and times especially for areas with food insecurity. Zimbabwe is considered to have a fragile food and nutrition security situation at both household and national levels for the past decade, mainly due to economic challenges, poor rainfall and erratic weather patterns resulting in reduced production of the main crops [37]–[39]. FAO once pointed out that the country as a whole lacks an overarching comprehensive agriculture policy framework and related sub-sectoral strategies [40]. This was due to the fact that the existing policy implementation was not contributing significantly to improving the lives of the women and small-scale farmers [41]. Recently, Zimbabwe's Ministry of Agriculture published a first draft of the nation's agriculture policy framework (2018-2030) [42]. Timely and accurate information regarding cropland extent is crucial for applications in the sectors of food security, agricultural monitoring, water management, modeling of land-use change and earth systems [27], [43].

Zimbabwe currently lacks reliable data on the extent of the re-allocated and new areas under cultivation [30]. In addition, there are no spatially explicit cropland products available showing the spatial extent of cropland areas [44] for Zimbabwe. The country suffers from inescapable cloud cover problem especially during the crop growing season, hence mapping cropland distribution and extent in a timely, accurate and reliable way using optical satellite imagery with high to medium spatial resolution is a challenging task. As a result, further applications of the cropland maps such as change detection on the cropland among others are encumbered. This research is conducted in anticipation to prompt the establishment of a National Cropland Data Layer based on satellite remote sensing data and be part of an annual or bi-annual cropland inventory that can be adopted by the respective and relevant agriculture and policy making agencies. The objectives of this research are to map cropland through (i) automatic classification (ii) multi-classifier system (MCS) and implementation of decision-level fusion (iii) NDVI-BSI thresholding and to determine the spatiotemporal cropland changes by a post-classification area comparison method.

II. STUDY AREA

Zimbabwe is a landlocked country situated in the southern part of Africa, between Zambezi and Limpopo rivers (FIGURE 1). It borders Mozambique to the east and north-east, South Africa to the south, west and south-west is Botswana and Zambia to the north-west. The country lies between latitude 15.60° and 22.42° S and longitude 25.22° and 33.08° E. It covers an area of approximately 390 757 km^2 and has a total population of almost 16 million as of 2018 and a relatively high population growth rate of around 2.3% annually [45]. The agricultural production is lagging behind with a growth rate of less than 1% annually [46]. This connotes a deteriorating food security status quo for the country [46].

Zimbabwe has a tropical climate with different local disparities and is reliant on the rains brought by Indian Ocean monsoons (seasonal winds) [47], [48]. The climate follows a bimodal rainfall pattern and generally experiences three seasons notably: (i) a hot, wet summer commencing mid-November to March (ii) a cold, dry winter season from April to July (iii) a hot, dry spring season from August to mid-November. The country's highest rainfalls are usually recorded in the Eastern Highlands, whereas the hottest temperatures are experienced in the Zambezi valley.

Agriculture is the backbone of Zimbabwe's economy and underpins the economic, social and political lives of the majority of the people of Zimbabwe [47]. Of the 39 million hectares land cover of Zimbabwe, 33.3 million hectares were considered to be arable farming land as noted in the 1980 government documentation [49]–[51]. Trade Economics defined agricultural land as the share of land area that is arable, under permanent crops and under permanent pastures [52]. According to World Bank, Zimbabwe's agricultural land was about 16 200 000 Ha as of 2014 [52]. Although Zimbabwe is now considered to have only 4.3 million hectares of arable land, it is estimated that less than 3 million hectares are currently under cultivation [41], [53].

III. MATERIALS AND METHODS

A. DATA

1) SATELLITE DATA

Due to the inescapable cloud cover problem, two satellite sensor imageries are implemented for each of the years under investigation. The satellite imagery hosted on GEE implemented with corresponding date ranges and spatial resolution

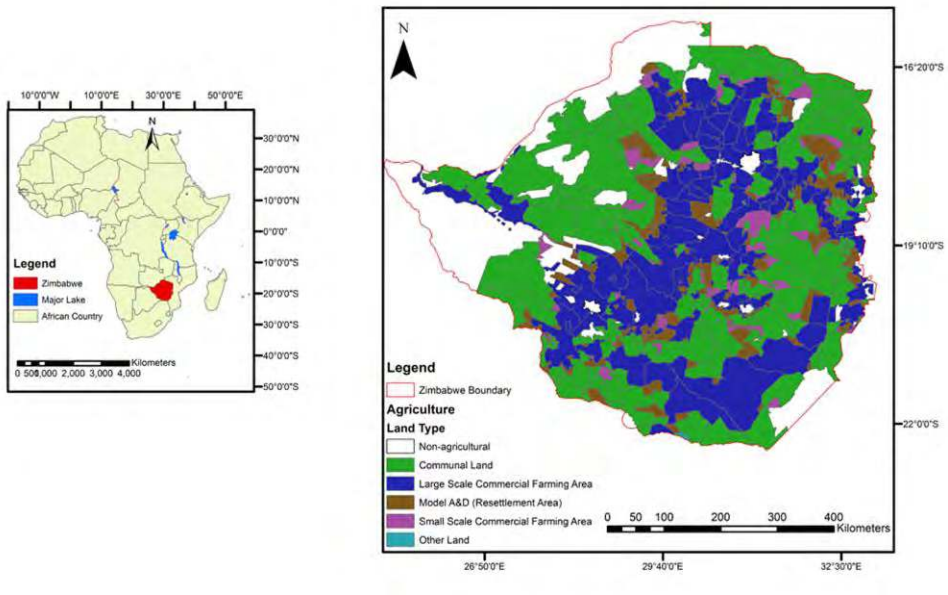

FIGURE 1. Study area Zimbabwe showing land tenure type and an inset showing location of Zimbabwe on the African continent.

TABLE 1. Image collections ID implemented and their purpose.

Year	Image Collection ID	Spatial resolution	Date range	Purpose
2001	LANDSAT/LT05/C01/T1_SR	30 m	01/01/2001 - 30/03/2001	Ensemble Classification and NDVI-BSI
	LANDSAT/LE07/C01/T1_SR	30 m		Ensemble Classification and NDVI-BSI
	LANDSAT/LT05/C01/T1	30 m	01/01/2001 - 30/03/2001	Automated classification
	LANDSAT/LE07/C01/T1	30 m	01/01/2001 - 30/03/2001	Automated classification
2007	LANDSAT/LT05/C01/T1_SR	30 m	01/01/2007 - 30/03/2007	Ensemble Classification and NDVI-BSI
	LANDSAT/LE07/C01/T1_SR	30 m		Ensemble Classification and NDVI-BSI
	LANDSAT/LT05/C01/T1	30 m	01/01/2007 - 30/03/2007	Automated classification
	LANDSAT/LE07/C01/T1	30 m	01/01/2007 - 30/03/2007	Automated classification
2013	LANDSAT/LE07/C01/T1_SR	30 m	01/01/2013 – 30/03/2013	Ensemble Classification and NDVI-BSI
	LANDSAT/LC08/C01/T1_SR	30 m	13/02/2013 - 30/04/2013	Ensemble Classification and NDVI-BSI
	LANDSAT/LE07/C01/T1	30 m	01/01/2013 – 30/03/2013	Automated classification
	LANDSAT/LC08/C01/T1	30 m	13/02/2013 - 30/04/2013	
2018	LANDSAT/LC08/C01/T1_SR	30 m	01/01/2018 - 30/03/2018	Ensemble Classification and NDVI-BSI
	COPERNICUS/S2	20 m		
	LANDSAT/LE07/C01/T1	30 m		Automated classification

are shown in TABLE 1. The peak of crop growing season in Zimbabwe falls between January and March/April, hence the choice of utilizing images captured in January, February and March.

Mosaics are created after masking out clouds from each image composite available using the median of the cloud-free pixels.

2) ANCILLARY DATA

a: DIGITAL ELEVATION MODEL (DEM)

Shuttle Radar Topography Mission (SRTM) 30 m resolution DEM is used to develop a slope map, and was downloaded from http://explorer.usgs.gov/. SOTER slope classes [54] are utilized as reference.

b: LAND USE SHAPEFILE

2010 Land use shapefile from Surveyor General (FIGURE 1), Zimbabwe, is used to clip areas where agricultural activities are expected to occur.

c: FOREST/NON-FOREST

Global PALSAR-2/PALSAR Forest/Non-Forest Map [55] for the years 2007, 2013 and 2017 are implemented to mask out forest areas. The raster layer is vectorized prior to masking out.

3) TRAINING AND VALIDATION DATA

a: AVAILABLE LULC REFERENCE MAPS AND CROPLAND DATA LAYERS

The U.S. Geological Survey (USGS) provides MODIS Land Cover Type product (MCD12Q1.006) data that characterize five global land cover classification systems at 500 m spatial resolution. MCD12Q1.006 data is available annually from 2001 to 2016. LC_Type 2 data is used as a source of training and validation data for automated classification in GEE. In GEE its image collection ID is MODIS/006/MCD12Q1.

An online cropland product derived by Xiong *et al.* [23] also called the Global Food Security-support Analysis Data at 30 m for the African Continent, Cropland Extent product (GFSAD30AFCE) is distributed through NASA's Land Processes Distributed Active Archive Center (LP DAAC) under the GFSAD30AFCE node on http://explorer.usgs.gov/ and/or can be found on https://croplands.org/app/map. The GFSAD30AFCE achieved a weighted overall accuracy

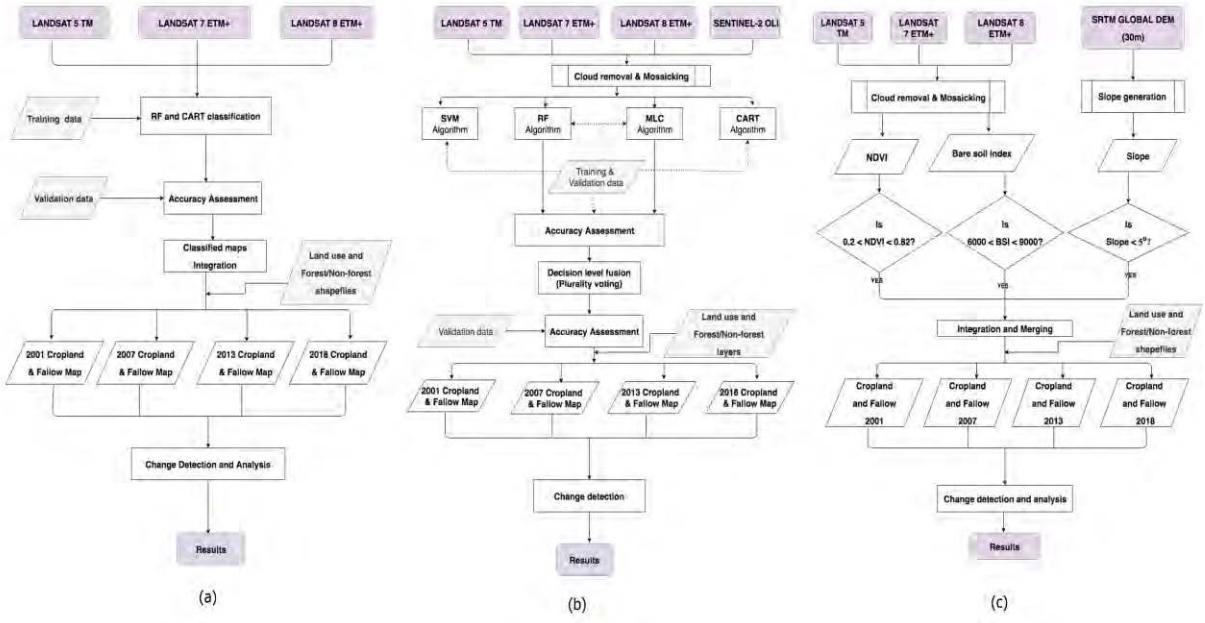

FIGURE 2. Generic flowchart of classification approaches implemented (a) automated classification (b) multi-classifier system (c) NDVI-BSI threshold.

of 94% when it was assessed against UN FAO statistics [23]. The interactive map or layer providing 30 m spatial resolution global cropland layer was used to manually select some samples used for training and validation purposes of MCS/ensemble classification in addition to the Global Navigation Satellite Systems (GNSS) collected samples. The cropland and non-cropland samples were also used for validation of NDVI-BSI threshold classification.

ESA's Land Cover Climate Change Initiative (CCI-LC) Climate Research Data Package (CRDP) contains 300 m spatial resolution land cover map products (2001, 2007, 2013 and 2015) whose cropland classes are utilized for comparison purposes with the cropland layers derived for 2001, 2007, 2013 and 2018 cropland layers respectively. The datasets are available on https://www.esa-landcover-cci.org/.

SADC Land Cover Dataset was produced and published by Environmentek, CSIR in 2002 in vector digital data format. The dataset was created at 1:250 000 scale from satellite imagery. It can be downloaded from http://gsdi.geoportal.csir.co.za/projects.

4) LOCAL KNOWLEDGE, PREVIOUS RESEARCH AND EXISTING LITERATURE

Some authors are relatively familiar with most of the cropland areas in Zimbabwe, their knowledge is also implemented in selecting the samples utilized for this research. Nonetheless, the selected samples are verified using the google earth images, GFSAD30AFCE interactive cropland layer and literature. The training and validation samples included samples implemented in previous researches on Zimbabwe crop mapping including Useya and Chen [48], Chemura *et al.* [56] are also adopted for this research.

Published articles including Hentze *et al.* [24], Sibanda and Murwira [57], Maguranyanga *et al.* [58], Makanza *et al.* [59], etc. are also adopted as reference data used for training dataset. Websites containing crops and croplands data utilized include http://zw.geoview.info, http://www.greenfuel.co.zw/, https://www.tangandatea.com/, https://www.bordertimbers.com/, etc.

5) GOOGLE EARTH

Samples obtained from the various sources are verified using Google Earth (http://earth.google.com). "*Google Earth contains an increasingly comprehensive image coverage of the globe at very high-resolution imagery (VHRI) 0.61–4 m allowing the user to have zoom-in-views (ZIV) into specific areas in great detail, from a base 30-m resolution data, based on GeoCover 2000*," [60].

B. METHODOLOGY

This research is conducted in three parts as represented by flowcharts in FIGURE 2. The figure illustrates (a) the automated classification (b) MCS (c) logical combination of NDVI-BSI threshold.

1) AUTOMATED CLASSIFICATION

Acquisition of reliable reference sample data from the ground or aerial photographs at or near the time of satellite overpass [61] can be a challenge which can also hinder automation of supervised classification techniques [31]. However, global LULC products can provide valuable information though they may have limited land use classes [31]. This approach is aimed at automating supervised

classification by utilizing MCD12Q1 product as the reference dataset since the optimum training size and distribution is typically anonymous for large area classification. MCD12Q1 provides annual land cover maps from 2001 to 2016, hence it is cost-effective and suitable for automatic classification approach in GEE.

The collections of raw Landsat 5, 7 and 8 scenes within the filtered date ranges (TABLE 1) are "*computed to Landsat top of atmosphere (TOA) in GEE by applying standard TOA calibration and then assigning a cloud score to each pixel using the SimpleLandsatCloudScore algorithm. Lowest possible range of cloud scores at each point are selected and then compute per-band percentile values from the accepted pixels. The algorithm also uses the LandsatPathRowLimit algorithm to select only the least-cloudy scenes in regions where more than maxDepth input scenes are available*," GEE.[2]

Random forest (RF) algorithm with 10 trees is used to downscale MODIS/006/MCD12Q1 to Landsat resolution. 1000 samples are randomly and automatically selected from the resampled MODIS/006/MCD12Q1 LC_Type 2 for the 10 classes namely; water, wetlands, croplands, urban, crop mosaic, barren, forest, shrub, grass and savannah. RF and classification and regression trees (CART) algorithms are employed separately for the automated classification approach. Cropland and crop mosaic classes are combined and extracted from the classified image to represent the cropland for Zimbabwe to be used for further analysis. Output croplands from the two Landsat sensors are aggregated into a single seamless layer.

2) MULTI-CLASSIFIER SYSTEM (MCS)

Satellite remote sensing potentially offers unswerving, timely resources that are expected to meet high scientific standards [60], but the inescapable cloud problem jeopardizes the quality of imagery provided. Endeavoring to improve the cloud-free spatial coverage, multi-sensor images are employed as data sources since their times of detecting and measuring the radiation that is reflected or backscattered from the target are different for each sensor. Therefore, the temporal resolution is increased indirectly hence maximizing on the cloud-free scenes that can be captured to compensate portions overwhelmed with clouds.

Various classifiers learn distribution patterns differently [48], multi-classifier system (MCS) and decision-level fusion (FIGURE 3) are employed to improve the quality of classified maps.

A good MCS must comprise classifiers which have complementary capabilities [48], [62]–[64] and exploit the redundant information [9]. The MCS comprises of CART [65], [66], support vector machines (SVM) [67] and RF [68] algorithms. 70% of the total randomly captured samples are used to train the classifiers whereas 30% are used for validation. 1500 samples are used for both training and validation.

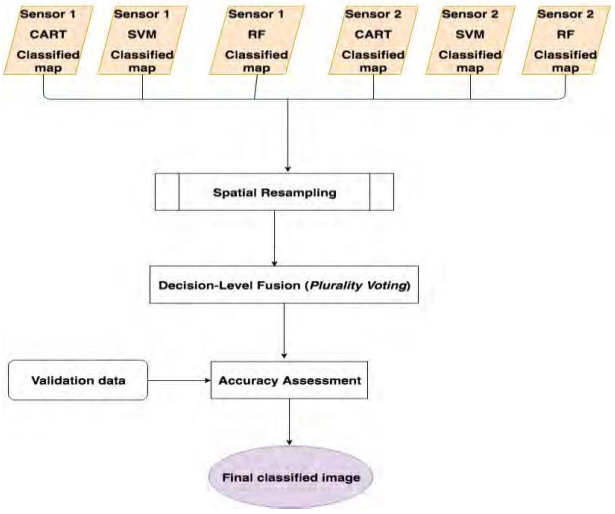

FIGURE 3. Multi-classifier system schema.

The classes discerned and their respective number of samples are waterbody (100), forest (100), fallow (100), bare (100), built-up (100), sugarcane (100), maize (75), coffee/tea (75), tobacco (75), banana (75), sorghum/millet (75), tomato (75), bean (75), groundnut (75), vegetable (75), pine (75), orchard fruits (apple, orange, avocado and macadamia nut) (75), and mixed (75).

Post-classification is performed to aggregate and mask cropland layer comprising fallow, sugarcane, maize, coffee/tea, tobacco, banana, sorghum/millet, tomato, bean, groundnut, vegetable, pine, orchard fruits, and mixed classes.

3) ACCURACY ASSESSMENT

Accuracy assessment is an important part of any classification project. It compares the classified image to another data source that is considered to be accurate or ground truth data. The evaluation can be performed in two forms namely qualitative and quantitative.

a: QUALITATIVE EVALUATION: VISUAL ASSESSMENT

For the classified images from the three approaches, visual evaluation is employed where each classified map is compared visually with google earth image and cropland layers. Some errors can be identified but the estimation of their sizes is dependent on the map user or producer.

b: QUANTITATIVE EVALUATION: ERROR/CONFUSION MATRIX

To quantitatively assess the accuracy of a classifier, an error or confusion matrix is an effective, standard descriptive tool implemented to organize and exhibit the thematic accuracy of a classified map [69]. A random 30% of captured samples are used for the accuracy assessment in ensemble classification scenarios employed.

[2] https://developers.google.com/earth-engine/api_docs

4) RESAMPLING

Resampling refers to a process whereby new pixel values are interpolated from existing values whenever the raster's structure is modified during cell resizing operation [70]. Images from different sensors need to be resampled such that the registration is accurate to subpixel locations [71]. Classified Sentinel-2 images are resampled to match spatial resolution of Landsat classified images, i.e. from 20 meters per pixel (mpp) to 30 mpp. The resampling process is implemented in ArcMap using the nearest neighbor (NN) interpolation algorithm aiming to minimize data integrity losses owing to the cell resizing since such resampling can have significant effects on the integrity of the data being compared [70]. NN is convenient because of its speed and ability to maintain the integrity of categorical data [70].

Root Mean Square Error (RMSE) is computed and implemented to assess the quality of the resampled dataset using (1).

$$RMSE = \sqrt{\sum_{i=1}^{n} \frac{[(X_i^{'} - X_i)^2 + \left(Y_i^{'} - Y_i\right)^2]}{n}} \quad (1)$$

where X_i'; Y_i' are coordinates of Ground Control Point(s) on resampled image, X_i; Y_i are coordinates of Ground Control Point(s) on reference image.

RMSE in the X coordinate = 0.001 m
RMSE in the Y coordinate = 0.013 m
Overall RMSE = 0.013 m

C. PLURALITY VOTING (DECISION-LEVEL FUSION)

Decision-level fusion merges the interpretations of different objects obtained from different source of information [64]. It is implemented in this paper to integrate the ensemble classified maps since it does not require prior knowledge about spectral configuration of the Landsat and Sentinel-2 [48]. Mandanici & Bitelli [72] discussed how Landsat 8 and Sentinel-2 can be integrated at pixel-level. Where more than a single map are to be overlaid, plurality voting [48], [73], [74] can be implemented to adopt the class to be incorporated into the ultimate classified map (FIGURE 3). This method is particularly successful when the classifiers involved output binary votes.

"*Thus by considering three classifiers: {C1, C2, C3}. Letting x be a new input example. If the three classifiers are identical, then when C1(x) provides a wrong classification, C2(x) and C3(x) will also provide erroneous results. If the errors made by the three classifiers are uncorrelated, the case might be that when C1(x) is wrong, C2(x) and C3(x) may be correct. In such a case, the majority vote amongst the three classifiers will correctly classify x.*"

Prior to the decision-level fusion, Sentinel-2 classified maps are resampled to 30 m spatial resolution and co-registered. Integrated classification is eventually assessed for its overall accuracy prior to post-classification change detection analysis.

1) SPECTRAL INDICES ALGEBRAIC COMBINATION USING NDVI AND BSI

Spectral indices enhance the spectral information and increase the separability of the LULC classes of interest thus enhancing the quality of the produced LULC map [75]. The spectral indices methods can have advantage over conventional multi-band spectral data classification. Both NDVI and BSI are pixel-based methods, easy to implement, though they require the user to determine at which threshold values are most suitable.

a: NDVI THRESHOLD ANALYSIS

NDVI is a spectral index that quantifies vegetation by measuring the difference between near-infrared (which vegetation strongly reflects) and red light (which vegetation absorbs) [76]. NDVI analysis give a rough sense of the photosynthetic activity within an area. NDVI values always ranges from −1 to +1, but there is no distinctive boundary for the different land cover types, actually, it depends on the image at hand and study area. The general rule is to test different threshold values and check image visually. NDVI is calculated on a pixel-based method using (2) [77].

$$NDVI = \frac{\rho_{NIR} - \rho_{Red}}{\rho_{NIR} + \rho_{Red}} \quad (2)$$

where ρ_{NIR} is surface reflectance value of near-infrared band and ρ_{Red} is surface reflectance value of red band.

NDVI values closer to +1 indicate dense vegetation, usually greener forests. On the other hand, low NDVI values designate less or no vegetation. Soils tend to generate rather small NDVI values approximately 0.1 – 0.2, negative NDVI values reflect potential water bodies. Nevertheless, there are some limitations such as sensitivity to soil and aerosols.

b: BARE SOIL INDEX (BSI) THRESHOLD ANALYSIS

BSI is a spectral index that enhances the identification of bare soil areas and fallow lands [78] depending on the soil characteristics. This index helps in separating the vegetation with different background types either completely bare or sparse canopy or dense canopy, etc. [79], [80]. As is the same with all indices, there is no distinct boundary for each type of land cover. Good human judgment, experience and prior knowledge of the study are crucial in order to select the best threshold values. BSI is calculated on a per-pixel basis using (3) [77], [81].

$$Bare\ Soil\ Index = \left[\frac{(\rho_{Red} + \rho_{SWIR}) - (\rho_{NIR} + \rho_{Blue})}{(\rho_{Red} + \rho_{SWIR}) + \rho_{NIR} + \rho_{Blue})}\right] \quad (3)$$

where ρNIR is surface reflectance value of near-infrared band and ρRed is surface reflectance value of red band, ρSWIR is surface reflectance value of shortwave-infrared band and ρBlue is surface reflectance value of blue band.

BSI increases as the bare soil exposure degrees of ground increase. Just like all other indices, not all surface soils have same color, presence or lack of organics, period since disturbance whether land clearing, wildfire, exposure due to infertile or dry soils.

2) SLOPE GENERATION

Downloaded 30 m spatial resolution SRTM DEM scenes are projected to UTM Zone 36S, WGS84 Datum, then mosaicked and further manipulated to derive slope map in degrees. The Slope tool calculates the maximum rate of change of elevation [82] from each cell to its neighboring cells, thus the tool fits a plane to the z-values of a 3 × 3 cell neighborhood around the processing or center cell in ArcGIS [83]. Basically, the maximum change in elevation over the distance between the cell and its eight neighbors identifies the steepest downhill descent from the cell [83].

3) CONDITIONAL MODEL

Conditional model in ArcMap is employed to integrate NDVI, BSI and slope maps. Raster calculator is the tool used (as shown in FIGURE 2 (c)) to delineate vegetation conditions and expose soil conditions. The following conditional statements are implemented.

$$\text{Con}((\text{“NDVI”} > 0.2)\ \&\ (\text{“NDVI”} < 0.85)\ \&\ (\text{“BSI”} > 6000)\ \&\ (\text{“BSI”} < 9000)\ \&\ (\text{Slope} < 5^{\circ}), 1, 0) \quad (4)$$

Croplands and fallow (pixels satisfying the conditions in (4) are re-coded to value 1 whereas any other classes are re-coded to value 0 and discarded. Land-use and non-forest layers are used to mask out the final cropland layer. Vegetation and bare soil have a highly negative correlation [80], [84]. Vegetation density can be calculated from using vegetation and bare soil indices as inputs [84].

D. CHANGE DETECTION ANALYSIS

Pre-classification and post-classification techniques are implemented to assess the changes occurring on the croplands. Each approach has its own pros and cons.

1) POST-CLASSIFICATION COMPARISON (CHANGE DETECTION STATISTICS)

The change detection statistical analysis is an efficient way of describing the changes observed [43] in the cropland class. The analysis chiefly focuses on the initial state classification changes to determine class-for-class image difference. The estimated cropland area or percentage statistics are derived from classified maps between successive years under investigation. The class changes are represented as percentages using (5). Positive change reflects an increase, whereas negative change depicts a decrease.

$$\frac{(\textit{final state} - \textit{initial state})}{\textit{initial state}} \times 100\% \quad (5)$$

IV. RESULTS

A. DESCRIPTIONS OF WHAT CONSTITUTES CROPLAND

TABLE 2 illustrates the description of what constitutes cropland class from ESA LC, this research, MCD12Q1, GFSAD30AFCE and SADC LC. Having a precise and clear definition of what is being mapped is vital prior to commencement of effective mapping. Endeavoring to minimize the cropland definition challenges, the common understanding from the definitions provided in TABLE 2 is that the standard definition must be compatible and relevant to remote sensing and in situ observations which incorporate as much of the diversity found within global agricultural systems as possible [85].

TABLE 2. Definitions of cropland.

Product	Description
ESA LC	Cropland rainfed Cropland irrigated or post-flooding Mosaic cropland (>50%) natural vegetation (<50%) Mosaic cropland (<50%) natural vegetation (>50%)
This paper	Cultivated crops/plants planted land Fallow Plantations
MCD12Q1	Croplands: at least 60% of area is cultivated cropland. Cropland/Natural Vegetation Mosaics: mosaics of small-scale cultivation 40-60% with natural tree, shrub, or herbaceous vegetation.
GFSAD30AFCE	Cultivated crops planted area and fallow lands “*lands cultivated with plants harvested for food, feed, and fiber, include both seasonal crops (e.g., wheat, rice, corn, soybeans, cotton) and continuous plantations (e.g., coffee, tea, rubber, cocoa, oil palms)*.”
SADC LC	Cultivation area- Areas of land that are ploughed and/or prepared for raising crops (excluding timber production). The category includes areas currently under crop, fallow land, and land being prepared for planting. Either no remaining natural vegetation cover, or severely impacted in most cases. Plantation area that are systematically planted, human-managed tree resources for commercial timber production but excludes non-timber based plantations such as tea, coffee, orchards used for citrus or nut crops.

B. CLASSIFICATION OVERALL ACCURACIES

Accuracy assessment of LULC maps constructed from remotely sensed data is crucial since it avails the data quality information to map users [69]. Various accuracy statistics can be computed from a confusion matrix. Nonetheless, there is no general consensus that has been reached on which measures are appropriate for a given objective of accuracy assessment, although the kappa statistic seems to be generally favored [69]. This research employs error matrices to determine both overall accuracies (OA) and kappa coefficients (KC) of classified maps. KC cogitates the whole error matrix instead of the diagonal elements as is the case with overall accuracy [48], [69].

Automated classification used MCD12Q1.006 as a source of training and validation data. The OA and KC for respective classifiers and satellite imagery are presented in TABLE 3. However, random forest produced relatively lower KC with respect to OA compared to CART algorithm. The KC are at odds with OA, there are discrepancies between the

TABLE 3. Classification accuracy of automated classification procedure. 1000 samples split into 70% training and 30% validation are used for 10 classes namely: water, wetlands, croplands, urban, crop mosaic, barren, forest, shrub, grass and savannah.

	2001		2007		2013		2018	
	Landsat 5	Landsat 7	Landsat 5	Landsat 7	Landsat 7	Landsat 8	Landsat 7	Landsat 8
RF	OA: 84.76% KC: 0.55	OA: 80.70% KC: 0.48	OA: 82.21% KC: 0.53	OA:82.12% KC: 0.54	OA:82.39% KC: 0.55	OA: 79.31% KC: 0.48	OA: 79.13% KC: 0.48	OA: 82.16% KC: 0.51
CART	OA: 93.81% KC: 0. 82	OA: 93.20% KC: 0.82	OA: 94.38% KC: 0.84	OA: 95.13% KC: 0.86	OA: 92.22% KC: 0.79	OA: 93.00% KC: 0.80	OA: 91.60% KC: 0.75	OA: 93.26% KC: 0.82

TABLE 4. Ensemble classification overall accuracies and fused product accuracy. A total of 1500 samples split into 70% training and 30% validation are used for 18 classes namely: waterbody, forest, fallow, bare, built-up, sugarcane, maize, coffee/tea, tobacco, banana, sorghum/millet, tomato, bean, groundnut, vegetable, pine, orchard fruits(apple, orange, avocado and macadamia nut), and mixed.

	2001		2007		2013		2018	
	Landsat 5	Landsat 7	Landsat 5	Landsat 7	Landsat 7	Landsat 8	Landsat 8	Sentinel-2
CART	OA: 75.49% KC: 0.68	OA: 85.58% KC: 0.81	OA:75.51 % KC: 0.68	OA: 69.92% KC: 0.61	OA: 72.40% KC: 0.64	OA: 76.15% KC: 0.68	OA: 84.11% KC: 0.80	OA:78.79 % KC: 0.76
SVM	OA:76.06 % KC: 0.68	OA: 85.19% KC: 0.81	OA:75.51 % KC: 0.68	OA: 71.32% KC: 0.62	OA: 72.40% KC: 0.64	OA: 76.15% KC: 0.68	OA: 86.27% KC: 0.82	OA: 78.49% KC: 0.76
RF	OA:75.31 % KC: 0.67	OA: 83.89% KC: 0.79	OA:76.35 % KC: 0.68	OA: 69.80% KC: 0.61	OA: 72.40% KC: 0.64	OA: 76.85% KC: 0.68	OA: 86.46% KC: 0.82	OA:78.63 % KC: 0.76
Fused	**OA: 87.23% KC: 0.84**		**OA:78.45 % KC: 0.75**		**OA: % 79.32 KC: 0.75**		**OA: 88.56% KC: 0.83**	

OA – overall accuracy
KC – kappa coefficient

two measurements. Probably one main reason why there is such a large difference between kappa and overall accuracy is that one of the discerned classes accounts for the large majority of the map. Kappa coefficient is a supplementary measure to overall accuracy, and at times, both are highly correlated, such that reporting kappa is redundant with overall accuracy. There is no direct relationship between KC and overall accuracy as they increase, and it depends on the marginal proportions [86]. The KC are sensitive to sample size [87]. Rossiter [86] highlighted that kappa statistics at times maybe difficult to explain to map users.

CART classified maps are adopted for further analysis and the RF classified images are disregarded.

C. ENSEMBLE CLASSIFICATION RESULTS

MCS consisting of CART, SVM and RF are implemented together with 1500 randomly selected samples split into 70% training and 30% validation, and their OAs and respective KC are presented in TABLE 4. Eventually, the plurality voting method is used to fuse the classified maps. On all cases, the fused seamless map produced higher OAs and KCs.

In 2001, Landsat 7 imagery produced better overall classification accuracy for all the classifiers than Landsat 5. Compared to 2007 classification accuracies, Landsat 5 performed better than Landsat 7. This is probably due to the reduce quality of image because of failure of Scan Line Corrector (SLC) which compensates for the forward motion of Landsat 7 that occurred since the 31st of May, 2003. For 2013, Landsat 8 performed better than Landsat 7, whereas in 2018, Landsat 8 performed better than Sentinel-2. The quality of Sentinel-2 imagery is severely affected by clouds. However, the fused seamless classified images produced higher overall accuracy than the ensemble classifiers for all the years. Useya & Chen [48] research also found that ensemble classifiers produce better overall classification accuracies, and the same has been proved by this research.

D. RELATIONSHIP BETWEEN NDVI AND BSI

2-D scatterplots are applied to interactively examine the structure of the data contained by NDVI and BSI bands. Upon plotting NDVI against BSI, the 2-band clusters relate to image properties (the land use classes), an inverse relationship can be apprehended. FIGURE 4 shows the 2013 2-D scatterplot of all pixels in the image. The 2-D scatterplots represent only the data in the main window, therefore different land-use classes produce a different scatterplot. For this research, very dense vegetation (forests) have relatively low BSI values and very high NDVI values. Waterbodies correspond to both lowest NDVI and BSI. Cropland lies between NDVI range 0.2 – 0.82 and BSI range 6000 – 9000. When combined with slope data, areas corresponding to slope less than 5° are most likely to be cropland.

E. VISUAL ASSESSMENT AND COMPARISON

Validation of the cropland maps synthesized through the approaches aforementioned is further aided by expert visual assessment with support of high-resolution images available on ESRI world imagery. Some locations are randomly selected and analyzed visually.

FIGURE 5(a), (b) and (d) depict Chisumbanje sugarcane estate as represented by the classified maps from the three approaches implemented and FIGURE 5(e) is GFSAD30AFCE cropland layer representing same site. FIGURE 5(a) shows under-representation by the automated

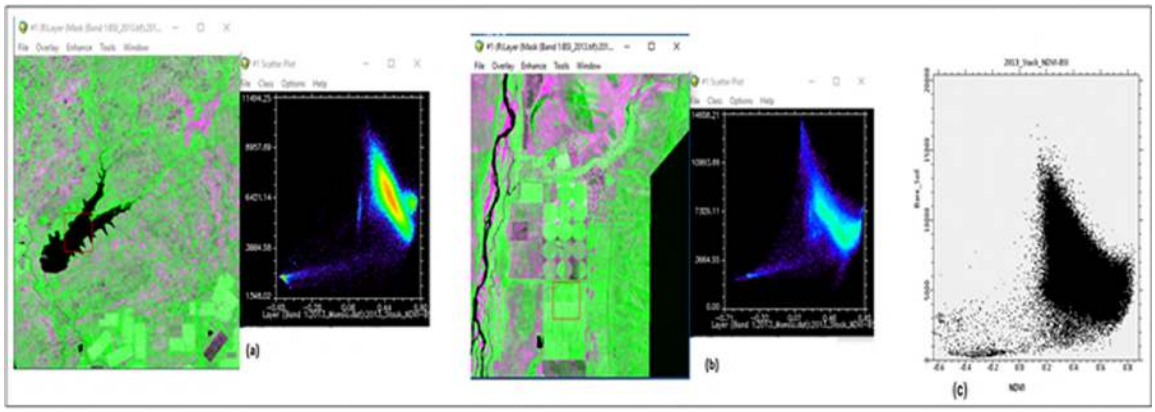

FIGURE 4. Screen shots when choosing the optimal threshold values for NDVI-BSI approach.

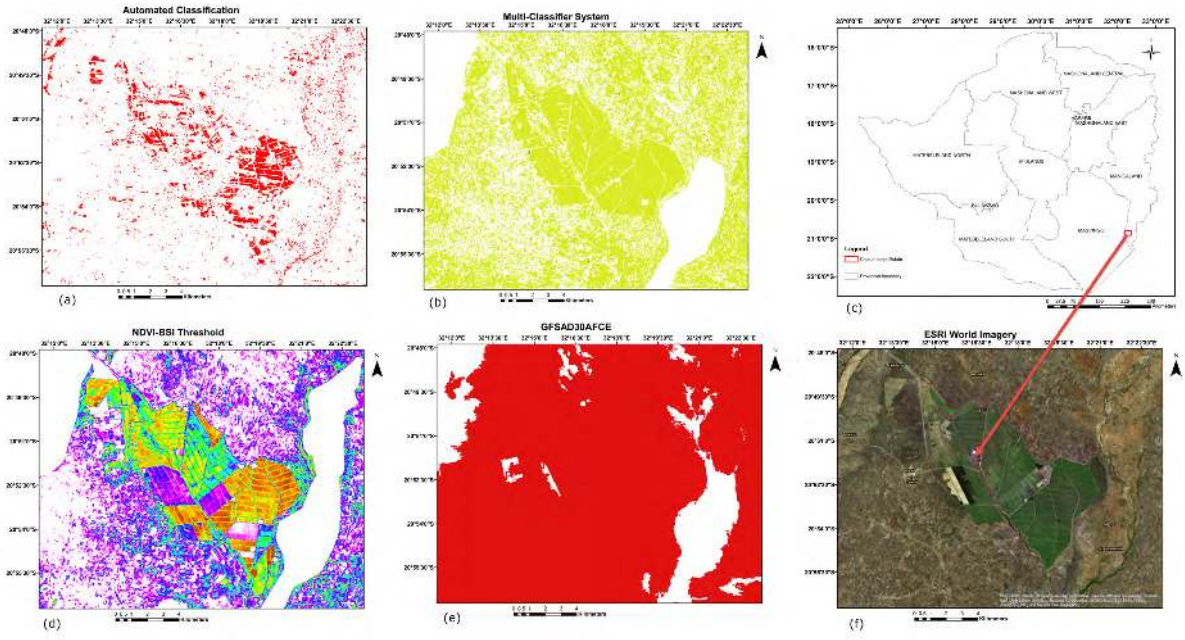

FIGURE 5. Chisumbanje sugarcane estate as presented by (a) automated classification approach (b) MCS approach (d) NDVI-BSI approach (e) GFSAD30AFCE cropland layer (f) ESRI world imagery. (c) is an inset of Zimbabwe showing the location of Chisumbanje Estate.

classification technique whereas FIGURE 5(e) reveals some over-representation by the GFSAD30AFCE cropland layer. Agricultural field parcels of a different land tenure type surround the sugarcane estate. The field patches are relatively small, hence are not distinctively classified. Nonetheless, the multi-classifier system shows better representation of the three classification techniques.

FIGURE 6 (a), (b) and (d) shows a fallow area as represented by the classified maps from the three approaches employed. The automated classification under-estimates the fallow area (FIGURE 6(a)). NDVI-BSI threshold technique (FIGURE 6 (b)) represents fairly better than the ensemble classification method (FIGURE 6 (d)) since it captures well the stream near middle of FIGURE 6(f). GFSAD30AFCE cropland layer over-estimates the fallow area (FIGURE 6 (e)).

From the visual assessment, MCS produced better results than NDVI-BSI thresholding approach. Automated classification severely under-estimated the cropland.

F. CROPLAND AREA COMPARISON

FIGURE 7 depicts cropland areal comparison between the methods explored. Automated classification method that utilized MCD12Q1.006 layer recorded the lowest cropland areas of the three approaches employed for the four years under investigation. The observed cropland area ranged from 3017617.92 to 4221719.52 Ha.

MCS cropland area ranges from 9 763 951 Ha to 10 793 606 Ha whereas the NDVI-BSI thresholding approach measured cropland areas ranges from 9 223 020 Ha to 10 482 323 Ha. The 2015 Zimbabwean cropland from the

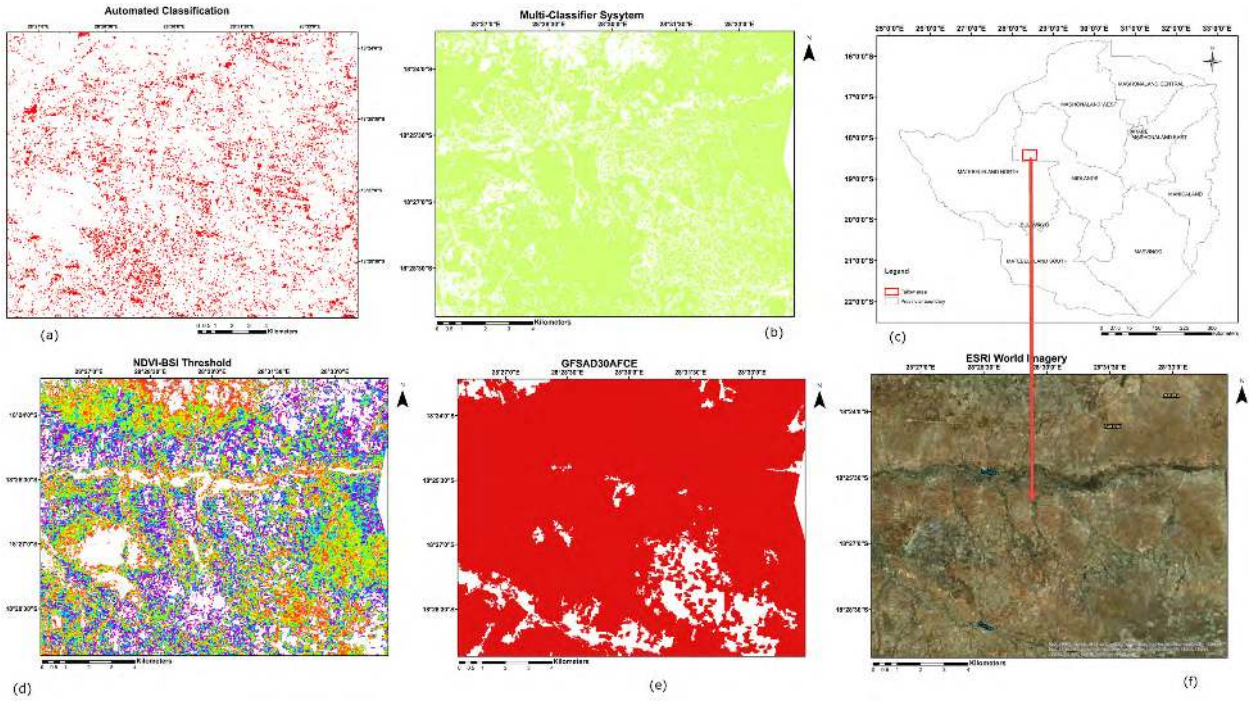

FIGURE 6. Fallow area as presented by (a) automated classification approach (b) MCS approach (d) NDVI-BSI approach (e) GFSAD30AFCE cropland layer (f) ESRI world imagery. (c) is an inset of Zimbabwe showing the location of fallow area.

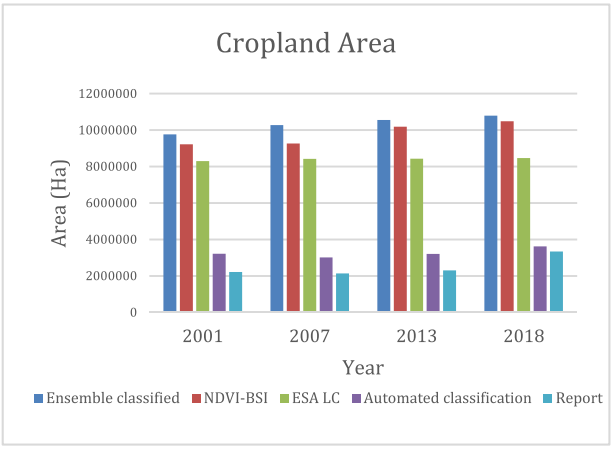

FIGURE 7. Total extracted cropland areas.

GFSAD30AFCE Cropland layer had a total area of 10 691 861.67 hectares, whereas SADC LC, cropland class had approximately 10 865 641.130 Ha in 2002.

Compared to the extracted values from the three classification methods implemented, the two cropland layers are matching closer with areas extracted from the ensemble and NDVI-BSI threshold approaches.

According to Trade Economics [52], agricultural land in Zimbabwe occupies almost 16 320 000 Ha, but arable land is estimated to be 10.34% of total Zimbabwe land area i.e. about 4 300 000 Ha. Zimbabwe's ministry of Agriculture, Mechanization and Irrigation Development [88], [89] keeps records on crop planted areas from crop censuses which are conducted yearly. The total planted areas are also included in FIGURE 7. The remote sensing extracted values are much higher than those in the ministry's records though the censuses do not necessarily include plantations and minor crops.

ESA LC cropland layer recorded cropland areas of approximately 8 301 789 Ha in 2001, 8 425 152 Ha in 2007, 8 433 198 Ha in 2013 and 8 465 283 Ha in 2015. These areas are less than areas from GFSAD30AFCE 2015's cropland layer and SADC's LC.

From the cropland areas comparison both MCS and NDVI-BSI approaches have comparable results though NDVI-BSI values are lower than MCS.

G. CHOOSING BEST APPROACH

The automatic classification approach despite having the best classification accuracies, the visual assessment and the areal comparison show under-representation of cropland areas. Overall accuracies for MCS and NDVI-BSI for 2013 are 80.54% and 79.32% respectively and for 2018 are 87.90% and 88.56% respectively. Their visual assessment results are comparable, hence both methods have their own pros and cons depending on the selected location. For cropland areal comparison, MCS produced higher areas than NDVI-BSI logical combinations thresholding approach.

In addition, FIGURE 8 shows the relationship between the extracted cropland areas for the 10 provinces in Zimbabwe from the MCS and NDVI-BSI thresholding approaches for 2013 and 2018. The strongest relationship is between

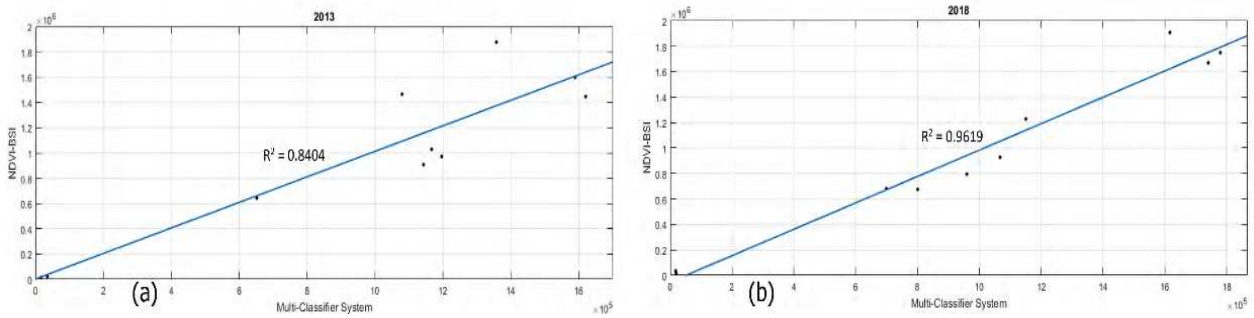

FIGURE 8. Relationship between ensemble classification and NDVI-BSI for years (a) 2013 (b) 2018.

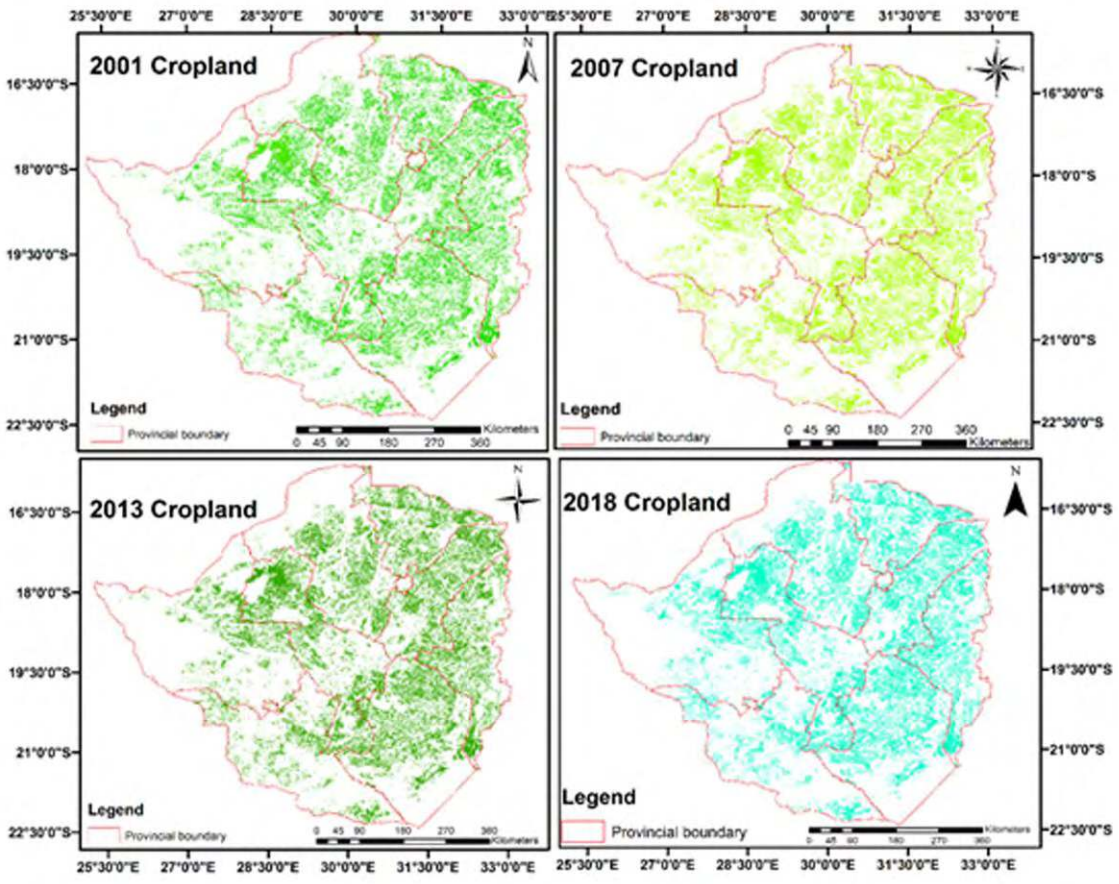

FIGURE 9. NDVI-BSI threshold cropland distribution maps for 2001, 2007, 2013 and 2018.

2018 croplands areas with a coefficient of determination (R^2) of 0.9619. 2013 extracted areas have an $R^2 = 0.8404$.

It is crucial to determine whether the relationships between croplands' areas extracted are statistically significant. F-test is performed on the croplands' areas for 2013 and 2018 and we obtained p-values of 0.7801 and 0.8725 respectively. The achieved p-values are both greater than 0.05, therefore the variables are not statistically significant. The linear regression models are statistically suitable to represent croplands from both MCS and NDVI-BSI at national-level.

FIGURE 9 shows final seamless cropland maps for 2001, 2007, 2013, and 2018 from NDVI-BSI thresholding approach.

H. STATISTICAL CHANGE DETECTION

TABLE 5, TABLE 6 and TABLE 7 present the statistical thematic change dynamics results from post classification using MCS approach for years under investigation respectively, where initial state classes are the column data and the final state classes are the row data. Row for image difference

TABLE 5. Statistics of percentage changes that occurred since 2001 to 2007.

		2001				
		Forest	Cropland	Bare	Built-up	Waterbody
2007	Background	0.57%	0.05%	0.96%	0.72%	4.49%
	Forest	**93.55%**	1.20%	2.81%	0.06%	1.30%
	Cropland	3.05%	**96.25%**	3.75%	1.50%	0.65%
	Bare	0.15%	0.85%	**88.81%**	1.92%	0.00%
	Built-up	2.60%	1.60%	3.02%	**95.70%**	0.00%
	Waterbody	0.08%	0.05%	0.65%	0.10%	**93.56%**
	Class total	100%	100%	100%	100%	100%
CROPLAND AREAL CHANGES						
2001		9763951 Ha			512 607.43 Ha **(5.25%)**	
2007		10276558.43 Ha				

TABLE 6. Statistical percentage changes that occurred between 2007 and 2013.

		2007				
		Forest	Cropland	Bare	Built-up	Waterbody
2013	Background	1.11%	0.88%	0.16%	1.00%	0.23%
	Forest	**88.63%**	1.30%	0.94%	0.10%	0.78%
	Cropland	6.75%	**96.50%**	1.59%	0.20%	3.85%
	Bare	0.60%	0.20%	**96.08%**	1.03%	0.20%
	Built-up	2.88%	1.02%	1.14%	**97.67%**	0.50%
	Waterbody	0.03%	0.10%	0.09%	0.00%	**94.44%**
	Class total	100%	100%	100%	100%	100%
CROPLAND AREAL CHANGES						
2007		10276558.43 Ha			276 439.42 Ha **(2.69%)**	
2013		10552997.85 Ha				

depicts the direction of change that is, positive values show increase and negative values show decrease in land use class.

TABLE 5 reveals that from 2001 to 2007, 3.05% of the forest transitioned to cropland, whereas 2.60% changed to built-up area. Of the cropland class, 96.25% remained unchanged, whereas 1.20% and 1.60% of cropland class were converted to forest and built-up respectively. Of the bare class 2.81% transitioned to forest, 3.75% changed to cropland and 3.02% became built-up.

TABLE 6 shows that from 2007 to 2013, 6.75% of the forest changed to cropland, whereas 2.88% changed to built-up area. Of the cropland class, 96.50% remained unaltered, whereas 1.30% and 1.02% of cropland class were converted to forest and built-up respectively. Of the bare class, 0.94% transitioned to forest, 1.59% changed to cropland and 1.03% became built-up.

Table 8 reveals that from 2016 to 2018, 8.40% of the forest became cropland, whereas 0.60% changed to built-up area. Of the cropland class, 97.42% remained unchanged, whereas 0.92% and 1.48% of cropland class were converted to forest and built-up respectively. Of the bare class, 0.80% transitioned to forest, 1.05% changed to cropland and 0.93% became built-up.

FIGURE 10 is a sankey diagram illustrating the gross gains or losses information contained in TABLE 5, TABLE 6 and TABLE 7 between or amongst land classes. The transitional changes that have occurred since 2001 until 2018 show the dynamic behavior of land use classes. Percentage values on both sides indicate land use type to Zimbabwe's total surface area.

TABLE 7. Statistical percentage changes that occurred from 2013 to 2018.

		2013				
		Forest	Cropland	Bare	Built-up	Waterbody
2018	Background	0.30%	0.10%	0.02%	0.43%	0.13%
	Forest	**90.64%**	0.92%	0.80%	0.50%	0.58%
	Cropland	8.40%	**97.42%**	1.05%	0.88%	2.50%
	Bare	0.00%	0.00%	**97.19%**	1.00%	0.10%
	Built-up	0.60%	1.48%	0.93%	**97.17%**	0.81%
	Waterbody	0.06%	0.08%	0.01%	0.02%	**95.88%**
	Class total	100%	100%	100%	100%	100%
CROPLAND AREAL CHANGES						
2013		10552997.85			240 608.35 Ha **(2.28%)**	
2018		10793606.20				

V. DISCUSSION

This paper is aimed at producing cropland maps from high-moderate spatial resolution imagery and determining the changes that occurred since 2001 till 2018. Three approaches are employed namely (i) automated classification using MCD12Q1.006 as a source of training and validation data (ii) ensemble classification using randomly selected training and validation samples (iii) NDVI-BSI thresholding. There are uncertainties in the mapping of croplands as observed by the three methods not agreeing on the cropland extents and total areas extracted. Visual inspection analysis is implemented and it is observed that automated classification method under-estimated the croplands extent compared to the other two methods.

A. MAPPING CROPLANDS

From the cropland maps produced (FIGURE 9), smallholder farming is the most prevalent form of agriculture in Zimbabwe, classification and mapping of the heterogeneous small-scale croplands is possible using the aforementioned implemented approaches. However, there are some limitations associated with each approach. From the visual analysis, the automated classification methodology generally underestimated the locations visually explored. This is due to the quality of the source of training and validation data. However, there are uncertainties associated with the land cover labels of annual land cover maps highlighted by the producers. Reference data is critical when performing classification, hence this approach accentuates the necessity to create reliable local, nationwide land use inventory to promote automated classification techniques. Nonetheless, this methodology for generating cropland is automatic, consistent and repeatable.

Fritz *et al.* [90] and Hentze *et al.* [24] implemented RMSE to compare FAO's agricultural statistics with cropland areas from GLC-2000 minimum, GLC-2000 maximum, SAGE, MODIS minimum and MODIS maximum. 16 countries; Botswana, Burkina Faso, Central African Rep.,

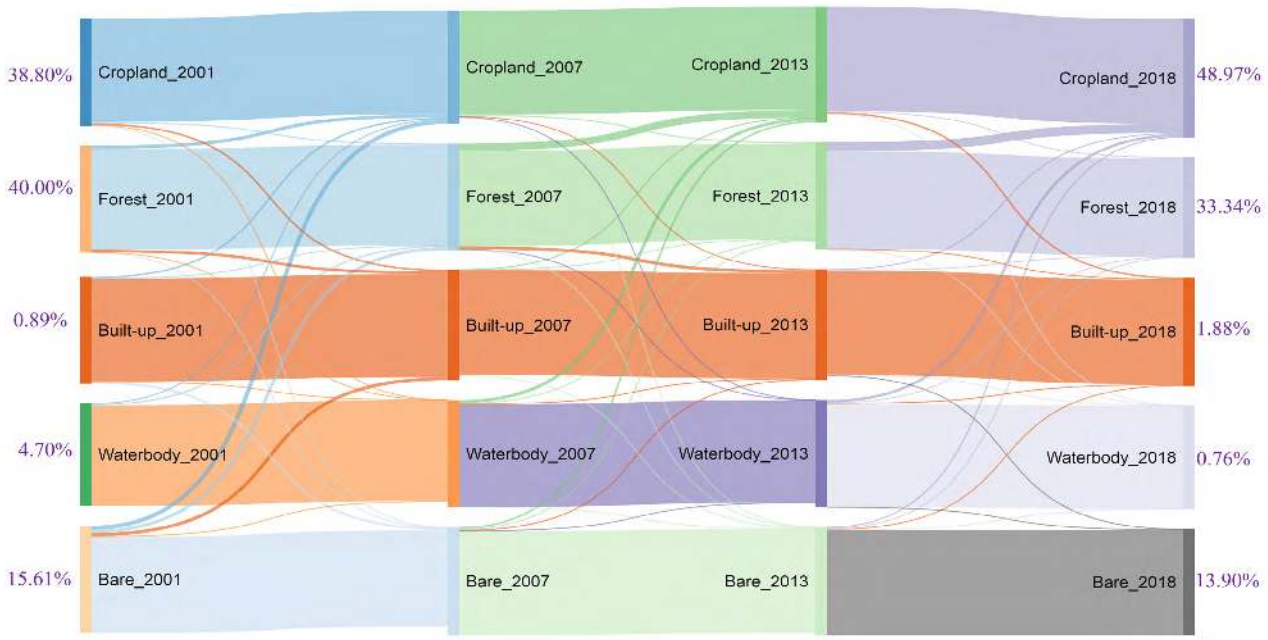

FIGURE 10. Sankey diagram showing the land use transitions from 2001 - 2007 - 2013 - 2013 - 2018 in Zimbabwe. Target node's color is used by the flow links between parallel columns. Class changes between successive nodes are indicated by the width of the link between the parallel columns. Percentage values on both sides indicate land use type to total area.

Chad, Eritrea, Gambia, Lesotho, Mali, Mauritania, Morocco, Namibia, Rwanda, Senegal, Somalia, Togo, and Zimbabwe were considered. The inevitable difference is due to the diverse methodologies and reference data utilized to derive the products. Reference data can be out-of-date or unreliable.

Selection and interpretation of the global LULC products need careful and comprehensive appraisal prior to use. The same observation pattern is revealed in this research. Spatially accurate crop mapping over large areas remains a bottleneck especially when implementing remote sensing.

Authors are recommending implementation of other spectral indices that can assist to promote automated cropland mapping. More exploration and exploitation of NDVI-BSI technique is recommended.

B. CHANGE DETECTION

Changes of cropland areas show a general increase (Tables 5, 6, and 7). Since the year 2000 there have been major changes in the agrarian economy of Zimbabwe due to the launch of the ''Fast track land reform'' programme which resulted in significant backward shifts in agricultural productivity [24], [91]. The agricultural land was redistributed to the black majority [39], [92], and this resulted in the existence of a lot of smallholder farmers. The annual population growth of 2.3% may explain the increase in cropland. The bigger the population the more food required to feed the growing population. Also in 2016/2017 farming season, the government of Zimbabwe re-introduced the ''command agriculture'' scheme where farmers were provide with farming inputs [93] hence explaining a further increase in the croplands in 2018.

C. CLIMATE DATA

Climate data was collected from Climate Change Knowledge Portal. FIGURE 11 shows average annual precipitation and temperature from 2000/2001 agriculture season to 2014/2015 season. 2000/2001 season recorded the highest annual precipitation and least mean annual temperature 2004/2005 season recorded the least annual precipitation and highest mean annual temperature.

In 2001/2002 agriculture season, most parts of southern Africa experienced a drought [49]. Zimbabwe experienced severe droughts during the 2005/2006 and 2009/2010 agricultural seasons, and the 2007/2008 season was the worst [94]. In February of 2016, Zimbabwe declared a 'state of disaster' due to drought worsened by the El Niño weather phenomenon which affected South Africa, Malawi and Zambia as well as Zimbabwe [95] and the same sentiments were expressed by Chisango [91] that the 2015/2016 season suffered a devastating drought.

However, during the 2016/2017 farming season, Zimbabwean government re-introduced the command agriculture scheme [48], [91], which can probably explain a rise in the cropland as show by TABLE 7. From the drought information, we can conclude that the planted areas information recorded by the ministry is definitely not the maximum potential for Zimbabwean farmers. There are many fallow areas being under-utilized, no crops are being grown.

There is a general increase in cropland area regardless the prolonged drought. Population increase and human activities are the main causes of cropland changes.

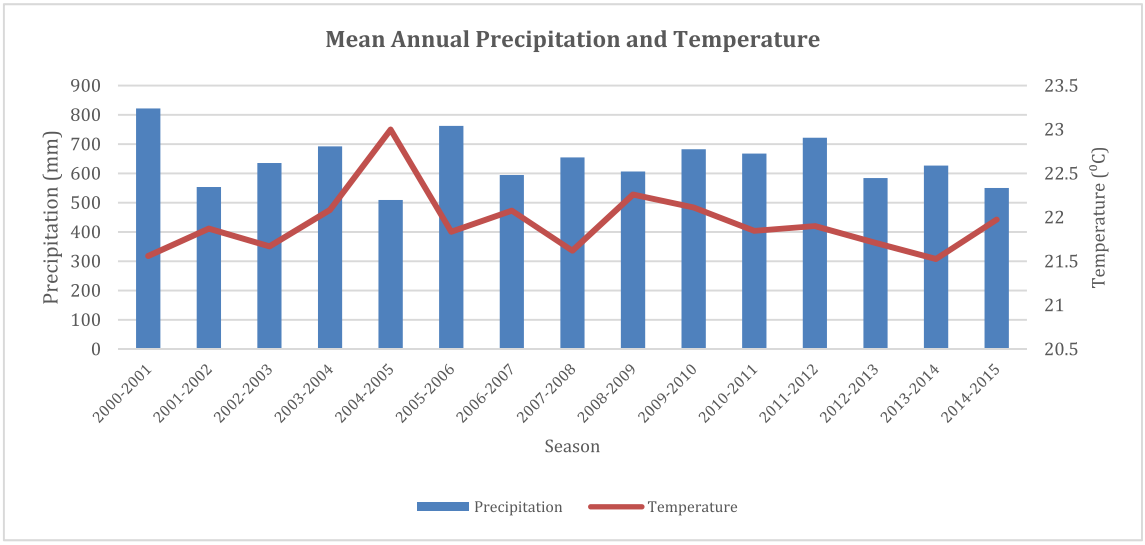

FIGURE 11. Average annual precipitation and temperature of Zimbabwe.

However, we recommend the implementation of cellular automata approach and agent-based simulation modeling to simulate the possible various changes happening on croplands since they have the capacity to include various variables that can better reflect and assist with forecasting.

D. WAY FORWARD

Performance of the NDVI-BSI thresholding approach is generally comparable with the performance of the MCS approach. The main disadvantage of MCS is that it requires good training and validation datasets, which in-turn is not a prerequisite for NDVI-BSI. The collection of training data can be cumbersome if not impossible or expensive.

The NDVI-BSI approach can easily be automated over time, once long-term evaluation is carried out, it allows synthesizing of relatively accurate and cheap cropland maps. Long-term cropland inventories can support detection and improve understanding of cropland changes.

Such automated accurate cropland mapping can be produced in GEE, a cloud-based geospatial processing platform. Reproduction of cropland maps can be done at any time, and the cost of production is very low. Monitoring of cropland areas can be promoted when NDVI-BSI thresholding approach is applied since the method is robust, consistent and repeatable.

VI. CONCLUSIONS

The objectives of this research are to map cropland by implementing (i) automatic classification (ii) ensemble classification and implementation of decision-level fusion (iii) NDVI-BSI thresholding and to determine the spatio-temporal cropland changes. Observations reveal that MCS and NDVI-BSI approaches performed better than automatic classification method, though there are inevitable uncertainties in the mapping of croplands. Cropland areas extracted from MCS and NDVI-BSI techniques are correlated with coefficient of determination of 0.8404 and 0.9619 for 2013 and 2018 respectively. MCS cropland areas are adopted for change detection since the extracted cropland areas are closer to the areas from SADC LC product and GFSAD30AFCE Cropland layer.

The automatic classification approach under-estimated the cropland extent despite having the highest overall classification accuracies. Automatic classification is implemented in Google Earth Engine and utilizes MCD12Q1.006 as a source of training and validation data. Random forest classification produced odd kappa coefficients with respect to the overall classification accuracies, hence CART classification results are adopted for further analysis.

Multi-classifier system comprising random forest, support vector machine and CART algorithms is employed. The ensemble classification utilizes randomly collected samples from other projects as training and validation data. Plurality voting method is applied to integrate individual classified maps. The decision-level fused map produced higher overall accuracies than individual classifiers.

NDVI-BSI obtained overall classification of 79.32% and 88.56% for 2013 and 2018 respectively. Visual inspection produced better representation than the MCS approach.

An average area of 10 346 778 Ha of cropland was determined. Whereas, NDVI-BSI thresholding technique produced an average of 9 788 833 Ha cropland area. SADC LC product's cropland layer of 2002 had an average of 10 865 641.130 Ha, whereas 2015 GFSAD30AFCE Cropland layer has a total area of 10 691 861.67 Ha.

From the post-classification change detection results, there is a general increase in cropland despite the prolonged drought experienced in the country. This cropland increase is due to human activities and population growth.

However, we recommend further analysis of the NDVI-BSI thresholding technique since it has more advantages than the MCS approach. These advantages include no need for prerequisite training datasets, the ability to automate easily and finally yet importantly, its robustness and rapidness in execution.

We also recommend simulation of cropland area changes using cellular automata and/or agent-based models to help to understand in detail the changes happening on croplands and forecast future changes.

ACKNOWLEDGMENT

The authors would like to thank the College of GeoExploration Science and Technology, and Jilin University for availing the resources, financial support and study environment.

REFERENCES

[1] *Agriculture at a Crossroads*, IAASTD, Berlin, Germany, 2016.
[2] J. A. Foley *et al.*, "Solutions for a cultivated planet," *Nature*, vol. 478, no. 7369, pp. 337–342, 2011.
[3] H. K. Gibbs *et al.*, "Tropical forests were the primary sources of new agricultural land in the 1980s and 1990s," *Proc. Nat. Acad. Sci. USA*, vol. 107, no. 38, pp. 16732–16737, 2010.
[4] H. Yu, B. Zhang, and Z. Wang, "Comparative study on changes of croplands between North Korea and South Korea during 1990–2015," *Chin. Geograph. Sci.*, vol. 28, no. 6, pp. 920–934, 2018.
[5] United Nations. Department of Economic and Social Affairs, Population Division. (2015). *World Population Projected to Reach 9.7 Billion by 2050*. Accessed: Dec. 24, 2018. [Online]. Available: http://www.un.org/en/development/desa/news/population/2015-report.html
[6] J. Chen, J. Chen, H. Liu, and S. Peng, "Detection of cropland change using multi-harmonic based phenological trajectory similarity," *Remote Sens.*, vol. 10, no. 7, p. 1020, 2018.
[7] J. Xiong *et al.*, "Automated cropland mapping of continental Africa using Google Earth Engine cloud computing," *ISPRS J. Photogramm. Remote Sens.*, vol. 126, pp. 225–244, Apr. 2017.
[8] J. O'Neil-Dunne, "Object-based approaches to data fusion land cover mapping," in *Proc. ASPRS*, Melbourne, VIC, Australia, 2017, p. 2.
[9] M. Schmitt and X. X. Zhu, "Data fusion and remote sensing: An ever-growing relationship," *IEEE Geosci. Remote Sens. Mag.*, vol. 4, no. 4, pp. 6–23, Dec. 2016.
[10] M. I. El-Gammal, R. R. Ali, and A. R. M. Samra, "NDVI threshold classification for detecting vegetation cover in Damietta governorate, Egypt," *J. Amer. Sci.*, vol. 10, no. 8, pp. 108–113, 2013.
[11] J. Deka, O. P. Tripathi, and M. L. Khan, "Study on land use/land cover change dynamics through remote sensing and GIS—A case study of Kamrup district, North East India," *J. Remote Sens.*, vol. 5, no. 1, pp. 55–62, 2014.
[12] R. S. Lunetta, J. F. Knight, J. Ediriwickrema, J. G. Lyon, and L. D. Worthy, "Land-cover change detection using multi-temporal MODIS NDVI data," *Remote Sens. Environ.*, vol. 105, no. 2, pp. 142–154, 2006.
[13] C. Gómez, J. C. White, and M. A. Wulder, "Optical remotely sensed time series data for land cover classification: A review," *ISPRS J. Photogramm. Remote Sens.*, vol. 116, pp. 55–72, Jun. 2016.
[14] M. D. Nellis, K. P. Price, and D. Rundquist, "Remote sensing of cropland agriculture," in *The SAGE Handbook of Remote Sensing*, vol. 1. Univ. of Nebraska–Lincoln, Nebraska: Papers in Natural Resources, 2009, pp. 368–380.
[15] N. Ramankutty, J. A. Foley, J. Norman, and K. McSweeney, "The global distribution of cultivable lands: Current patterns and sensitivity to possible climate change," *Global Ecol. Biogeogr.*, vol. 11, no. 5, pp. 377–392, 2002.
[16] J. B. Sharma, "Remote sensing education, research and outreach with the Google Earth engine," in *Proc. ASPRS*, Melbourne, VIC, Australia, 2017, p. 4.
[17] (2018). *Cloud Computing With Amazon Web Services*. Accessed: Dec. 20, 2018. [Online]. Available: https://aws.amazon.com/what-is-aws/
[18] A. Mellor, "The Impact of training data characteristics on ensemble classification of land cover," Ph.D. dissertation, RMIT Univ., Melbourne, VIC, Australia, 2017.
[19] R. Sugumaran, J. W. Hegeman, V. B. Sardeshmukh, and M. P. Armstrong, "Processing remote-sensing data in cloud computing environments," in *Remotely Sensed Data Characterization, Classification, and Accuracies*, vol. 1. Boca Raton, FL, USA: CRC Press, 2015, pp. 549–556.
[20] C. Zhu, D. Lu, D. Victoria, and L. V. Dutra, "Mapping fractional cropland distribution in Mato Grosso, brazil using time series MODIS enhanced vegetation index and landsat thematic mapper data," *Remote Sens.*, vol. 8, no. 1, pp. 1–22, 2015.
[21] B. S. Nguh and N. B. Maluh, "The implications of land use/cover dynamics on resources development in Tubah sub-division, Cameroon," *J. Archit. Eng. Technol.*, vol. 06, no. 02, 2017.
[22] S. Azzali and M. Menenti, "Mapping vegetation-soil-climate complexes in southern Africa using temporal Fourier analysis of NOAA-AVHRR NDVI data," *Int. J. Remote Sens.*, vol. 21, no. 5, pp. 973–996, 2000.
[23] J. Xiong *et al.*, "Nominal 30-m cropland extent map of continental Africa by integrating pixel-based and object-based algorithms using sentinel-2 and landsat-8 data on Google Earth engine," *Remote Sens.*, vol. 9, no. 10, p. 1065, 2017.
[24] K. Hentze, F. Thonfeld, and G. Menz, "Evaluating crop area mapping from MODIS time-series as an assessment tool for Zimbabwe's 'fast track land reform programme,"' *PLoS ONE*, pp. 1–22, 2016.
[25] ESA-Landcover-CCI. (2017). *Climate Research Data Package (CRDP)*. Accessed: Feb. 5, 2019. [Online]. Available: http://maps.elie.ucl.ac.be/CCI/viewer/download.php
[26] E. Bartholomé and A. S. Belward, "GLC2000: A new approach to global land cover mapping from Earth observation data," *Int. J. Remote Sens.*, vol. 26, no. 9, pp. 1959–1977, Feb. 2007.
[27] F. Waldner, S. Fritz, A. Di Gregorio, and P. Defourny, "Mapping priorities to focus cropland mapping activities: Fitness assessment of existing global, regional and national cropland maps," *Remote Sens.*, vol. 7, no. 6, pp. 7959–7986, 2015.
[28] O. Arino, P. Bicheron, F. Achard, J. Latham, R. Witt, and J.-L. Weber, "GLOBCOVER: The most detailed potrait of Earth," Eur. Space Agency, Paris, France, Tech. Rep. Bulletin 136, 2008.
[29] M. A. Friedl *et al.*, "Global land cover mapping from MODIS: Algorithms and early results," *Remote Sens. Environ.*, vol. 83, nos. 1–2, pp. 287–302, 2002.
[30] C. Vancutsem, E. Marinho, F. Kayitakire, L. See, and S. Fritz, "Harmonizing and combining existing land cover/land use datasets for cropland area monitoring at the African continental scale," *Remote Sens.*, vol. 5, no. 1, pp. 19–41, 2012.
[31] H. K. Zhang and D. P. Roy, "Using the 500 m MODIS land cover product to derive a consistent continental scale 30 m landsat land cover classification," *Remote Sens. Environ.*, vol. 197, pp. 15–34, Aug. 2017.
[32] K. J. Wessels *et al.*, "Rapid land cover map updates using change detection and robust random forest classifiers," *Remote Sens.*, vol. 8, no. 11, p. 8888, 2016.
[33] J. Radoux, C. Lamarche, E. Van Bogaert, S. Bontemps, C. Brockmann, and P. Defourny, "Automated training sample extraction for global land cover mapping," *Remote Sens.*, vol. 6, no. 5, pp. 3965–3987, 2014.
[34] K. Jia *et al.*, "Land cover classification of landsat data with phenological features extracted from time series MODIS NDVI data," *Remote Sens.*, vol. 6, no. 11, pp. 11518–11532, 2014.
[35] P. Gong *et al.*, "Finer resolution observation and monitoring of global land cover: First mapping results with landsat TM and ETM+ data," *Int. J. Remote Sens.*, vol. 34, no. 7, pp. 2607–2654, 2013.
[36] Harris Geospatial Solutions. (2018). *Change Detection Analysis*. Accessed: Jan. 4, 2019. [Online]. Available: https://www.harrisgeospatial.com/docs/ChangeDetectionAnalysis.html
[37] USAID, Agriculture and Food Security. (2018). *Food Assistance Fact Sheet—Zimbabwe*. Accessed: Dec. 27, 2018. [Online]. Available: https://www.usaid.gov/zimbabwe/food-assistance
[38] WFP. (2018). *Zimbabwe: Zero Hunger*. Accessed: Dec. 27, 2018. [Online]. Available: http://www1.wfp.org/countries/zimbabwe
[39] S. Wiggins, "Food security options in Zimbabwe: Multiple threats, multiple opportunities?" Overseas Develop. Inst., London, U.K., Tech. Rep. 5, 2004.
[40] T. Mutenga, "Zimbabwe lacks comprehensive agriculture policy," Commercial Farmers Union Zimbabwe, Harare, Zimbabwe, Tech. Rep., 2018. Accessed: Jan. 22, 2019. [Online]. Available: http://www.cfuzim.org/index.php/agriculture/11543-zimbabwe-lacks-comprehensive-agriculture-policy

[41] J. Echanove, "Food security, nutrition, climate change resilience, gender and the small-scale farmers: Zimbabwe," CARE Int., Harare, Zimbabwe, Tech. Rep., 2017.
[42] *National Agriculture Policy Framework (2018-2030): First Draft*, Government Zimbabwe, Harare, Zimbabwe, 2018.
[43] U. Renu, R. K. Nema, M. K. Awasthi, and Y. K. Tiwari, "Change detection analysis of Cropland using geospatial technique—A case study of narsinghpur district," *Int. J. Environ., Agricult. Biotechnol.*, vol. 2, no. 4, pp. 1726–1731, 2017.
[44] L. H. Samberg, J. S. Gerber, N. Ramankutty, M. Herrero, and P. C. West, "Subnational distribution of average farm size and smallholder contributions to global food production," *Environ. Res. Lett.*, vol. 11, no. 12, p. 124010, 2016.
[45] World Bank. (2019). *Zimbabwe Population Growth Annual Percent—Trading Economics*. Accessed: Feb. 7, 2019. [Online]. Available: https://tradingeconomics.com/zimbabwe/population-growth-annual-percent-wb-data.html
[46] V. W. P. Van Engelen, S. Mantel, J. A. Dijkshoorn, and J. Huting, "The impact of desertification on food security in Southern Africa: A case study in Zimbabwe," UNEP Wageningen, The Netherlands, Tech. Rep. FP/1000-02-0-2201, 2004.
[47] A. A. Maiyaki, "Zimbabwe's agricultural industry," *African J. Bus. Manage.*, vol. 4, no. 19, pp. 4159–4166, 2010.
[48] J. Useya and S. Chen, "Comparative performance evaluation of pixel-level and decision-level data fusion of landsat 8 OLI, landsat 7 ETM+ and sentinel-2 MSI for crop ensemble classification," *IEEE J. Sel. Top. Appl. Earth Observ. Remote Sens.*, vol. 11, no. 11, pp. 4441–4451, Nov. 2018.
[49] M. Mutasa, "Zimbabwe's drought conundrum: Vulnerability and coping in Buhera and Chikomba districts," M.S. thesis, Dept. Int. Environ. Develop. Stud. (Noragric), Norwegian Univ. Life Sci., Ås, Norway, 2010.
[50] M. Tekere, J. Hurungo, and M. Rusare. Zimbabwe. FAO. Accessed: Jan. 22, 2019. [Online]. Available: http://www.fao.org/docrep/005/y4632e/y4632e0y.htm#fn114
[51] T. Mabaye, "Land Reform in Zimbabwe: An examination of past and present policy short comings and successes and recommendations for improvement," Tech. Rep., 2005.
[52] Trade Economics. (2019). *Zimbabwe Agriculture*. Accessed: Jan. 23, 2019. [Online]. Available: https://tradingeconomics.com/zimbabwe/agricultural-land-sq-km-wb-data.html
[53] H. C. Sadza, C. M. Nherera, T. Nhenga-Chakarisa, J. Tagwireyi, and M. Munyuki-Hungwe, "Executive summary: Zimbabwe zero hunger," Women's Univ. in Africa, Harare, Zimbabwe, Tech. Rep., 2015.
[54] *Atlas of SOTER-Derived Maps of Zimbabwe. Impact of Desertification on Food Security*, ISRIC, Wageningen, The Netherlands, 2005, pp. 1–54.
[55] M. Shimada *et al.*, "New global forest/non-forest maps from ALOS PALSAR data (2007–2010)," *Remote Sens. Environ.*, vol. 155, pp. 13–31, Dec. 2014.
[56] A. Chemura, O. Mutanga, and J. Odindi, "Empirical modeling of leaf chlorophyll content in coffee (Coffea Arabica) plantations with sentinel-2 MSI data: Effects of spectral settings, spatial resolution, and crop canopy cover," *IEEE J. Sel. Topics Appl. Earth Observ. Remote Sens.*, vol. 10, no. 12, pp. 5541–5550, 2017.
[57] M. Sibanda and A. Murwira, "The use of multi-temporal MODIS images with ground data to distinguish cotton from maize and sorghum fields in smallholder agricultural landscapes of Southern Africa," *Int. J. Remote Sens.*, vol. 33, no. 16, pp. 4841–4855, 2012.
[58] C. Maguranyanga, A. Murwira, and M. Sibanda, "Distinguishing maize, soyabean and tobacco fields using temporal MODIS 16 day NDVI images in the large scale commercial farming areas of Zimbabwe," *J. Indian Soc. Remote Sens.*, vol. 43, no. 1, pp. 79–87, 2015.
[59] R. Makanza *et al.*, "High-throughput phenotyping of canopy cover and senescence in maize field trials using aerial digital canopy imaging," *Remote Sens.*, vol. 10, no. 2, p. 330, 2018.
[60] P. S. Thenkbail *et al.*, "Global irrigation area mapping (GIAM) and statistics using remote sensing," in *Remote Sensing of Global Croplands for Food Security*, P. S. Thenkabail, J. G. Lyon, T. Hugh, and B. Chandrashekhar, Eds. Indianapolis, IN, USA: CRC Press, 2009, pp. 41–117.
[61] C. Kamusoko and M. Aniya, "Hybrid classification of landsat data and GIS for land use/cover change analysis of the Bindura district, Zimbabwe," *Int. J. Remote Sens.*, vol. 30, no. 1, pp. 97–115, 2008.
[62] T. Matsuyama, "Knowledge-based aerial image understanding systems and expert systems for image processing," *IEEE Trans. Geosci. Remote Sens.*, vol. GRS-25, no. 3, pp. 305–316, May 1987.
[63] Y. I. Lu, "Knowledge integration in a multiple classifier system," *Appl. Intell.*, vol. 6, no. 2, pp. 75–86, 1996.
[64] F. Samadzadegan, "Data integration related to sensors, data and models," in *Proc. ISPRS Conf.*, 2004, pp. 1–6.
[65] L. Breiman, J. Friedman, C. J. Stone, and R. A. Olshen, *Classification and Regression Trees*. London, U.K.: Taylor & Francis, 1984.
[66] L. Breiman, *Classification and Regression Trees*. Evanston, IL, USA: Routledge, 2017.
[67] C. J. C. Burges, "A tutorial on support vector machines for pattern recognition," *Data Mining Knowl. Discovery*, vol. 2, no. 2, pp. 121–167, 1998.
[68] L. Breiman, "Random forest," *Mach. Learn.*, vol. 45, no. 1, pp. 5–32, 2001.
[69] S. V. Stehman, "Selecting and interpreting measures of thematic classification accuracy," *Remote Sens. Environ.*, vol. 62, no. 1, pp. 77–89, 1997.
[70] H. Studley and K. Weber, "Comparison of image resampling techniques for satellite imagery," Tech. Rep., 2011. [Online]. Available: https://pdfs.semanticscholar.org/fa31/6fc18b22fe466f818bcea0edae76d08c91f9.pdf
[71] J. A. Parker, R. V. Kenyon, and D. Troxel, "Comparison of interpolating methods for image resampling," *IEEE Trans. Med. Imag.*, vol. 2, no. 1, pp. 31–39, Mar. 1983.
[72] E. Mandanici and G. Bitelli, "Preliminary comparison of sentinel-2 and landsat 8 imagery for a combined use," *Remote Sens.*, vol. 8, no. 12, p. 1014, 2016.
[73] X. Zhang, X. Feng, and W. Ke, "Integration of classifiers for improvement of vegetation category identification accuracy based on image objects," *New Zeal. J. Agricult. Res.*, vol. 50, no. 5, pp. 1125–1133, 2007.
[74] X. Lin, S. Yacoub, J. Burns, and S. Simske, "Performance analysis of pattern classifier combination by plurality voting," *Pattern Recognit. Lett.*, vol. 24, no. 12, pp. 1959–1969, 2003.
[75] M. Ustuner, F. B. Sanli, S. Abdikan, M. T. Esetlili, and Y. Kurucu, "Crop type classification using vegetation indices of rapideye imagery," *Int. Arch. Photogram., Remote Sens. Spatial Inf. Sci.*, vol. 40, no. 7, pp. 195–198, 2014.
[76] GISGeography. (2018). *What is NDVI (Normalized Difference Vegetation Index)*. Accessed: Jan. 22, 2019. [Online]. Available: https://gisgeography.com/ndvi-normalized-difference-vegetation-index/
[77] W. Chen, L. Liu, C. Zhang, J. Wang, J. Wang, and Y. Pan, "Monitoring the seasonal bare soil areas in Beijing using multitemporal TM images," in *Proc. IEEE Int. Geosci. Remote Sens. Symp. (IGARSS)*, vol. 5, no. 3, Sep. 2004, pp. 3379–3382.
[78] Brecht. (2018). *Remote Sensing Indices—Regen Network–Medium*. Accessed: Dec. 13, 2018. [Online]. Available: https://medium.com/regen-network/remote-sensing-indices-389153e3d947
[79] P. S. Roy, K. P. Sharma, and A. Jain, "Stratification of density in dry deciduous forest using satellite remote sensing digital data—An approach based on spectral indices," *J. Biosci.*, vol. 21, no. 5, pp. 723–734, 1996.
[80] A. Rikimaru and S. Miyatake, "Development of forest canopy density mapping and monitoring model using indices of vegetation, bare soil and shadow," in *Proc. 18th Asian Conf. Remote Sens. (ACRS)*, 1997, p. 3.
[81] Z. Azizi, A. Najafi, and H. Sohrabi, "Forest canopy density estimating using satellite images," *Int. Arch. Photogramm. Remote Sens. Spat. Inf. Sci.*, vol. 37, no. B8, p. 4, 2008.
[82] P. A. Burrough, R. McDonnell, R. A. McDonnell, and C. D. Lloyd, *Principles of Geographical Information Systems*, 3rd ed. New York, NY, USA: Oxford Univ. Press, 2015.
[83] ESRI. (2016). *How Slope Works ArcMap: ArcGIS for Desktop*. Accessed: Jan. 11, 2019. [Online]. Available: http://desktop.arcgis.com/en/arcmap/10.3/tools/spatial-analyst-toolbox/how-slope-works.htm
[84] M. Sahana, H. Sajjad, and R. Ahmed, "Assessing spatio-temporal health of forest cover using forest canopy density model and forest fragmentation approach in Sundarban reserve forest, India," *Model. Earth Syst. Environ.*, vol. 1, no. 4, p. 49, 2015.
[85] *JECAM Guidelines for Cropland and Crop Type Definition and Field Data Collection*, JECAM, Brussels, Belgium, 2014, pp. 1–7.
[86] D. G. Rossiter, "Statistical methods for accuracy assesment of classified thematic maps," Dept. Earth Syst. Anal., Univ. Twente, Fac. Geo-Inf. Sci., Earth Observ., Enschede, The Netherlands, 2004.
[87] A. J. Viera and J. M. Garrett, "Understanding interobserver agreement: The kappa statistic," *Family Med.*, vol. 37, no. 5, pp. 360–363, 2005.
[88] *First Round Crop and Livestock Assessment Report (2016-2017)*, MAM Development, Harare, Zimbabwe, 2017.
[89] *First Round Crop and Livestock Assessment Report (2008-2009)*, MAM Development, Harare, Zimbabwe, 2009.

[90] S. Fritz, L. See, F. Rembold, S. Fritz, L. See, and F. Rembold, "Comparison of global and regional land cover maps with statistical information for the agricultural domain in Africa," *Int. J. Remote*, vol. 31, no. 9, pp. 2237–2256, 2010.
[91] T. F. F. Chisango, "Challenges and prospects of Zimbabwe's command farming in unlocking the country's smallholder agricultural economy," *Int. J. Agric. Econ.*, vol. 3, no. 4, pp. 76–82, 2018.
[92] I. MacNairn, "Food security brief," USAID, Washington, DC, USA, Tech. Rep., Mar. 2014, pp. 1–52. [Online]. Available: http://fews.net/sites/default/files/documents/reports/Zimbabwe_Food_Security_Brief_2014_0.pdf
[93] T. Mutenga, "Command agric misses target," *The Financial Gazette, Harare*, p. 1, Aug. 2017.
[94] G. Mutowo and D. Chikodzi, "Remote sensing based drought monitoring in Zimbabwe," *Disaster Prevention Manage.*, vol. 23, no. 5, pp. 649–659, 2014.
[95] A. France-Presse. (2016). Zimbabwe declares 'state of disaster' due to drought. The Guardian. Accessed: Jan. 21, 2019. [Online]. Available: https://www.theguardian.com/world/2016/feb/05/zimbabwe-declares-state-of-disaster-drought-robert-mugabe

JULIANA USEYA received the B.Sc. degree (Hons.) in geoinformatics and surveying from the University of Zimbabwe, in 2007, the M.Sc. degree in geoinformatics from the Faculty of ITC, University of Twente, in 2011. She is currently pursuing the master's degree with the Department of Remote Sensing and GIS, College of Geo-Exploration Science and Technology, Jilin University, China. Her research interests include multi-sensor classification, agricultural remote sensing, and synthetic aperture radar application techniques.

SHENGBO CHEN received the Ph.D. degree in earth exploration and information technology, in 2000. He is currently a Full Professor with the College of Geo-Exploration Science and Technology, Jilin University. His current research interests include applications of remote sensing in geology, agriculture, and exploration of the lunar systems.

MIKE MUREFU received the bachelor's degree in geoinfomatics and surveying engineering from the University of Zimbabwe, in 2013. He is a currently pursuing the master's degree in cartography and geographic information engineering with the College of Geo-Exploration Science and Technology, Jilin University. His current research interests include the application of UAVs in crop health monitoring and the use of Google Earth Engine in solving remote sensing big data problems, such as monitoring multi-decadal wetlands change dynamics in Africa.